AD-A123 859 MIXED CONDUCTION IN SEMI-INSULATING GALLIUM ARSENIDE 1/1
(U) ARMY ELECTRONICS RESEARCH AND DEVELOPMENT COMMAND
FORT MONMOU.. J J WINTER ET AL. DEC 82 DELET-TR-82-12

UNCLASSIFIED F/G 20/10 NL

END
DATE FILMED
3-83
DTIC

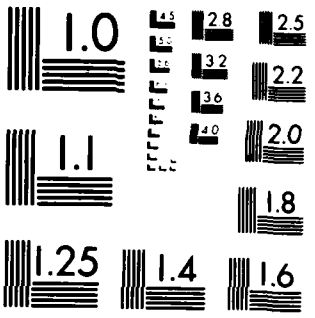

RESEARCH AND DEVELOPMENT TECHNICAL REPORT

DELET-TR-82-12

AD A123859

MIXED CONDUCTION IN SEMI-INSULATING GALLIUM ARSENIDE

J. J. WINTER
H. A. LEUPOLD
R. L. ROSS
A. BALLATO

ELECTRONICS TECHNOLOGY & DEVICES LABORATORY

DECEMBER 1982

ERADCOM

US ARMY ELECTRONICS RESEARCH & DEVELOPMENT COMMAND
FORT MONMOUTH, NEW JERSEY 07703

NOTICES

Disclaimers

The citation of trade names and names of manufacturers in this report is not to be construed as official Government indorsement or approval of commercial products or services referenced herein.

Disposition

Destroy this report when it is no longer needed. Do not return it to the originator.

UNCLASSIFIED

SECURITY CLASSIFICATION OF THIS PAGE (When Data Entered)

REPORT DOCUMENTATION PAGE	READ INSTRUCTIONS BEFORE COMPLETING FORM
1. REPORT NUMBER DELET-TR-82-1? 2. GOVT ACCESSION NO. AD-A123859	3. RECIPIENT'S CATALOG NUMBER
4. TITLE (and Subtitle) MIXED CONDUCTION IN SEMI-INSULATING GALLIUM ARSENIDE	5. TYPE OF REPORT & PERIOD COVERED
	6. PERFORMING ORG. REPORT NUMBER
7. AUTHOR(s) J. J. Winter, H. A. Leupold, R. L. Ross, A. Ballato	8. CONTRACT OR GRANT NUMBER(s)
9. PERFORMING ORGANIZATION NAME AND ADDRESS US Army Electronics Research & Development Command Fort Monmouth, NJ	10. PROGRAM ELEMENT, PROJECT, TASK AREA & WORK UNIT NUMBERS 61102A 1L161102AH47 02 051
11. CONTROLLING OFFICE NAME AND ADDRESS US Army Electronics REsearch & Development Command Fort Monmouth, NJ 07703 DELET-ES-S	12. REPORT DATE December 1982
	13. NUMBER OF PAGES 20
14. MONITORING AGENCY NAME & ADDRESS(if different from Controlling Office)	15. SECURITY CLASS. (of this report) UNCLASSIFIED
	15a. DECLASSIFICATION/DOWNGRADING SCHEDULE

16. DISTRIBUTION STATEMENT (of this Report)

Approved for public release; distribution unlimited.

17. DISTRIBUTION STATEMENT (of the abstract entered in Block 20, if different from Report)

18. SUPPLEMENTARY NOTES

A

19. KEY WORDS (Continue on reverse side if necessary and identify by block number)

gallium arsenide, compensation, mixed conduction, Shockley diagrams, semi-insulating

20. ABSTRACT (Continue on reverse side if necessary and identify by block number)

Hall effect and conductivity measurements made on semi-insulating bulk GaAs are examined by a new approach to mixed conduction analysis. Based on Fermi level and electron mobility analyses of conductivity and Hall coefficient, it uses revised values of effective densities of states at the band edges, and electron/hole mobility ratios recently adopted by other workers. The treatment provides a visual analysis of the system in terms of the electrical parameters and impurity densities, and establishes criteria for the onset of mixed conduction.

DD FORM 1 JAN 73 1473 EDITION OF 1 NOV 65 IS OBSOLETE

UNCLASSIFIED

SECURITY CLASSIFICATION OF THIS PAGE (When Data Entered)

CONTENTS

TABLES

FIGURES

MIXED CONDUCTION IN SEMI-INSULATING GALLIUM ARSENIDE

INTRODUCTION

With the ever-increasing use of gallium arsenide in a wide variety of integrated circuits and millimeter-wave/microwave devices, a demand has arisen for reproducible semi-insulating substrate material for device fabrication. Synthesis of such material has been hampered by an incomplete and sometimes erroneous knowledge of its transport properties, and the impurity states by which they are affected. Especially troublesome has been the difficulty in separating the contributions of electrons and holes in the range of Fermi levels where neither carrier dominates conduction, that is, the mixed conduction region (MCR). An early attempt at a solution met with some success,[1,2] but was found inadequate for many samples since it neglected single carrier magneto-resistance and magneto-Hall effects. A new version developed a family of curves relating electron mobility to Hall mobility through resistivity.[3] That analysis and those employed by other workers rest on assumptions or semi-empirical deductions about the electron/hole mobility ratio in conjunction with either the intrinsic carrier concentration or the actual electron mobility. Divergent views of criteria establishing the MCR result, and these are masked in part by the different temperatures assumed in the various analyses. However, the adopted mobility ratios used in these analyses are similar, and can be used with established values of the energy gap and the effective densities of states at the band edges to form a more general and comprehensive analysis applicable at all reasonable temperatures. Accordingly, we have developed and used such an approach to analyze Hall and conductivity data taken on samples grown by the United States Army Electronics Technology and Devices Laboratory (ET&DL), as well as on specimens previously discussed by Martin.[4]

EXPERIMENTAL

The ET&DL specimens were grown by means of a modified liquid (molten B_2O_3) encapsulated Czochralski technique that employs in situ compounding and results in low silicon content (typically, 3×10^{14} at cm^{-3}).[5] The material was cut into Greek cross structures by ultrasonic milling, and contacted with tin, which was annealed at 450°C for 5 minutes in flowing hydrogen. Van der Pauw measurements of conductivity and Hall coefficient were made at room temperature with a fully guarded system capable of measuring conductivities of less than 10^{-12} Siemens/cm.[6,7]

THE BASIC EQUATIONS

In the absence of a magnetic field, the Hall coefficient is given by

$$R = (R_p\sigma_p^2 + R_n\sigma_n^2)/(\sigma_n + \sigma_p)^2 \qquad (1)$$

and the conductivity by

$$\sigma = \sigma_n + \sigma_p = ne\mu_n + pe\mu_p = \mu_n e\,(n + pb^{-1}) \qquad (2)$$

where e is the electron charge, μn and μp are the respective electron and hole concentrations, μn and μp their mobilities, and b their ratio μ_n/μ_p. The electron and hole Hall coefficients, R_p and R_n, may be written as $-r_n/ne$ and r_p/pe, respectively. The scattering factor, r, is very difficult to measure or calculate precisely. However, general considerations indicate that it usually does not vary

appreciably from unity,[3,8-12] nor substantially affect the outcome of solutions in the MCR. For the most general case, $(r_n \neq r_p)$, the Hall concentration is given by

$$H = r_n/Re = (n + (\mu_p/\mu_n)p)^2/(p\alpha^{-1}(\mu_p/\mu_n)^2-n) = (n + pb^{-1})^2/(p\alpha^{-1} b^{-2}-n) \quad (3)$$

while the Hall mobility μ_H, defined as $R\sigma$ is written in the form

$$\mu_H/\mu_n r_n = (p\alpha^{-1}(\mu_p/\mu_n)^2-n)/(n + p(\mu_p/\mu_n)) = (p\alpha^{-1}b^{-2}-n)/(n + pb^{-1}) \quad (4)$$

where $\alpha = r_n/r_p$. Also of interest is the ratio

$$\sigma/\sigma_n = 1 + (p/n)(\mu_p/\mu_n) = 1 + b^{-1}p/n \quad . \quad (5)$$

Away from the band edges, the electron and hole concentrations vary with Fermi energy E_f and temperature T as

$$n = N_c(\exp((E_g - E_f)/kT))^{-1} \text{ and} \quad (6)$$

$$p = N_v(\exp(E_f/kT))^{-1} \quad . \quad (7)$$

If the energy of the valence band edge E_v is taken to be zero, that of the conduction band edge E_c is then equal to the bandgap, E_g, which varies with temperature according to $E_g = 1.519 - (5.405 \times 10^{-4})\, T^2/(T + 204)$.[13] N_c and N_v are the effective densities of states at the conduction and valence band edges, respectively, and are given by $N_c = 8.80 \times 10^{13}\, T^{3/2}\, (1-T/4000)$ and $N_v = 1.66 \times 10^{15}\, T^{3/2}$ cm^{-3}.[14] To complete the set of equations needed to obtain the carrier concentrations and mobilities from experimental values of conductivity and Hall coefficient, a relationship between electron and hole mobility is necessary. At 400K, a constant electron/hole mobility ratio of

$$b = \mu_n/\mu_p = 15 \quad (8)$$

is used by Martin,[4] while at 295K the following empirical relationship is proposed by Look,[3]

$$b = \mu_n/\mu_p = 13 + 9X10^{-4}\mu_n \quad . \quad (9)$$

It is to be noted that these ratios are not very different for most observed mobilities. To facilitate comparisons of the present work with analyses made by Martin and Look, we will consider the case $\alpha = r_n/r_p = 1$ and use equations (8) and (9) for analyses of measurements made at 400K and 295K, respectively. In addition, discussion of the basic parameters and equations employed will be limited to values below the lattice-limited values of electron mobility, 6000 cm^2/Vs and 8000 cm^2/Vs at 400K and 295K, respectively.[1-3]

CONDUCTIVITY CRITERIA FOR THE ONSET OF MIXED CONDUCTION EFFECTS

A particularly illuminating and analytically convenient basis for the investigation of mixed conduction effects is obtained by plotting the variables σ, $r/|Re|$, n and p vs. the Fermi energy E_f on a semi-log graph, while observing lattice-limited mobility constraints. Conductivity and $r/|Re|$ are plotted for several values over the range of possible mobilities. There is only one $r/|Re|$ curve in Figures 1a and 1b, since the mobility ratio b is taken to be a constant here. In Figure 2, where b is a function of μ_n, there is a family of $r/|Re|$ curves. All of the foregoing plots appear as straight lines over most of their ranges, with any departures from linearity (that is, departures of σ from σ_n, σ_p and $r/|Re|$ from p,n) occurring only within the mixed conduction region. Such a graph affords a simple, visually obvious and accurate establishment of mixed conduction criteria, the boundaries of the MCR being the outer limits at which significant deviations from linearity occur for any curve. A deviation of $1/|Re|$ from n of about 8% is sufficiently small to serve as the criterion for such a boundary, yet discernible on graphs of reasonable size. The deviations of σ from $e\mu_n n$ at the boundaries are too small to be discernible (see Figure 1b for example). The conductivities associated with this criterion are 10^{-5} and 2×10^{-9} S/cm for temperatures of 400K and 295K, respectively. For conductivities above these values, equations 2-4 reduce to

$$\sigma \approx \sigma_n = \mu_n e n \tag{2A}$$

$$r/|Re| \approx n \tag{3A}$$

$$\mu_H = \approx r\mu_n \tag{4A}$$

and we have a solution for n in terms of the measured quantity R. Solutions for E_f and p follow from a consideration of Figure 1a. A glance at Figures 1a and 2 suffices to ascertain that for negative R, i.e., Fermi energies above the $R = 0$ line, mixed conduction effects are small for conductivities above the line NMC at about 6.4×10^{-6} and 1.7×10^{-9} Siemens/cm for temperatures of 400K and 295K, respectively. As shown in Figures 1b and 2, the NMC conductivity is defined by the intersection of the conductivity curve for the lattice-limited mobility and the $p = n$ line. This choice of criterion results in deviations of σ and μ_H from σ_n and μ_n of about 7% and of R from r/ne of 12%, which is sufficiently accurate for most analytical purposes. It has the additional advantage of providing easily recognizable graphical features to mark the onset of mixed conduction. The third, and perhaps most important, advantage afforded by this choice will be discussed on page 10. The region defined by the $p = n$ and $R = 0$ lines and labeled NRMCR, represents the MCR for negative R. In the next section we will expand upon the reason for associating the departure from linearity with the Fermi level where $p = n$. At this energy, the deviation of $1/|Re|$ from n is about 12%. Table 1 indicates how μ_H and σ differ from μ_n and σ_n, respectively, at this and other key Fermi energies for various values of b.

The conductivity of Martin's[4] sample C2 at 400K was about 2.4×10^{-5} Siemens/cm. Since this is appreciably above tne NMC line, mixed conduction effects are minimal, and the measured Hall mobility of 3200 cm^2/Vs should be a very good approximation to $r\mu_n$. Martin's estimate of $r\mu_n$ for this sample was 4500-5000 cm^2/Vs. The long arrows on Figure 1a indicate the system Fermi energies (E_{fs}) determined by the intersection of the dotted $(Re)^{-1}$ data line for C2(-4.6×10^{10} cm^{-3}) and the $r/|Re|$ curve where a scattering coefficient r of 1 has been assumed. The intersection of the

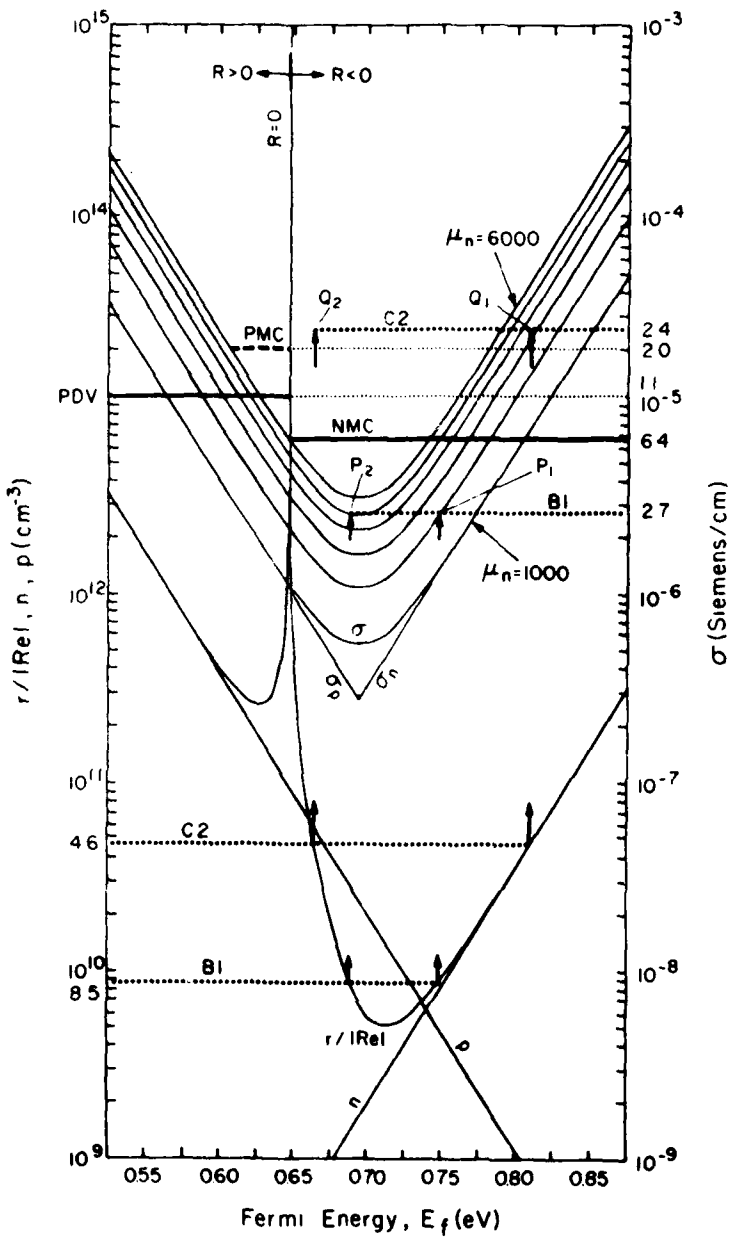

T=400K

$N_c = 6.34 \times 10^{17}$ cm^{-3}

$N_v = 1.33 \times 10^{19}$ cm^{-3}

$E_g = 1.376$ eV

$\frac{\mu_n}{\mu_p} = 15 = b$

$r_n = r_p = r$

$$\frac{r}{Re} = \frac{(n+pb^{-1})^2}{(n-pb^{-2})}$$

$$\sigma = \mu_n e(n+pb^{-1})$$

Figure 1a. Carrier Concentrations, Hall Concentration and Conductivity vs. Fermi, T=400K.

Carrier concentrations n,p, Hall concentration $r/|Re|$, and conductivity σ, as functions of Fermi level at 400K. The family of σ curves indicates how σ depends on electron mobility μ_n. Measurements from Samples C2 and B1, Table 3, are analyzed.

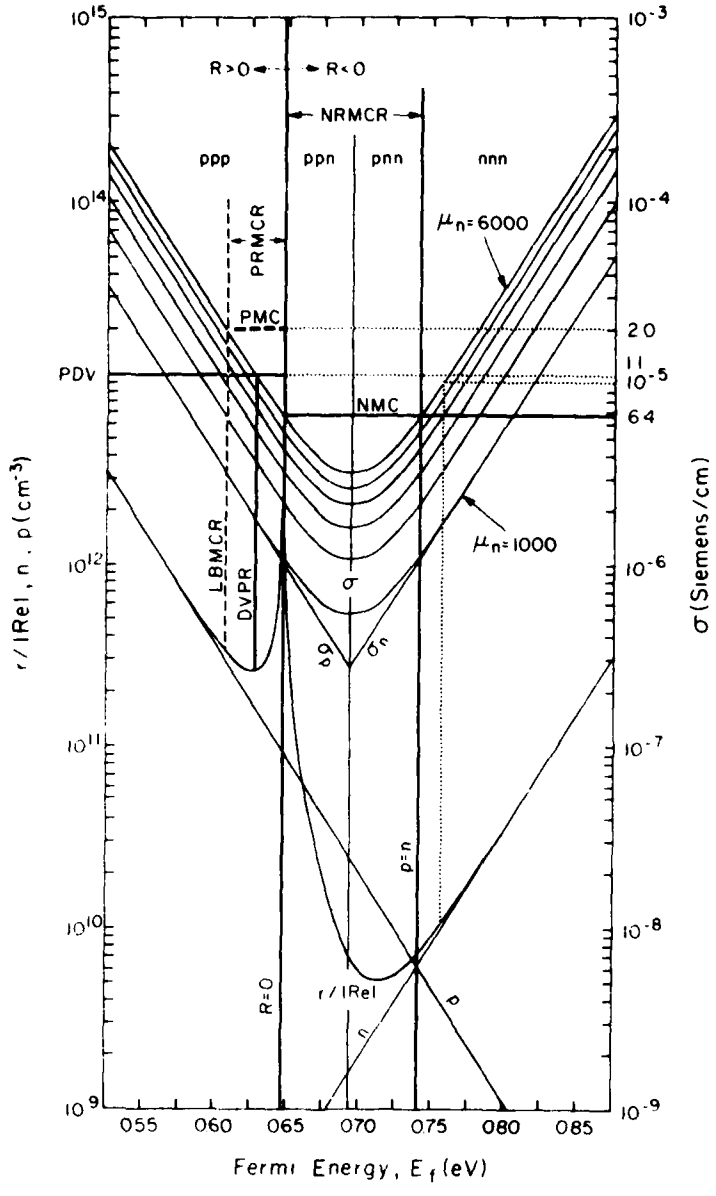

Figure 1b. Delineation of Mixed Conduction Regions for Positive and Negative Hall Coefficients, T=400K.

Same plots as in 1a, but the mixed conduction regions, PRMCR and NRMCR, for positive and negative R values are defined. Regions exhibiting different degrees of carrier dominance, e.g., nnn, are also delineated. The vertical dotted line marks the 8% deviation of r/|Re| from n.

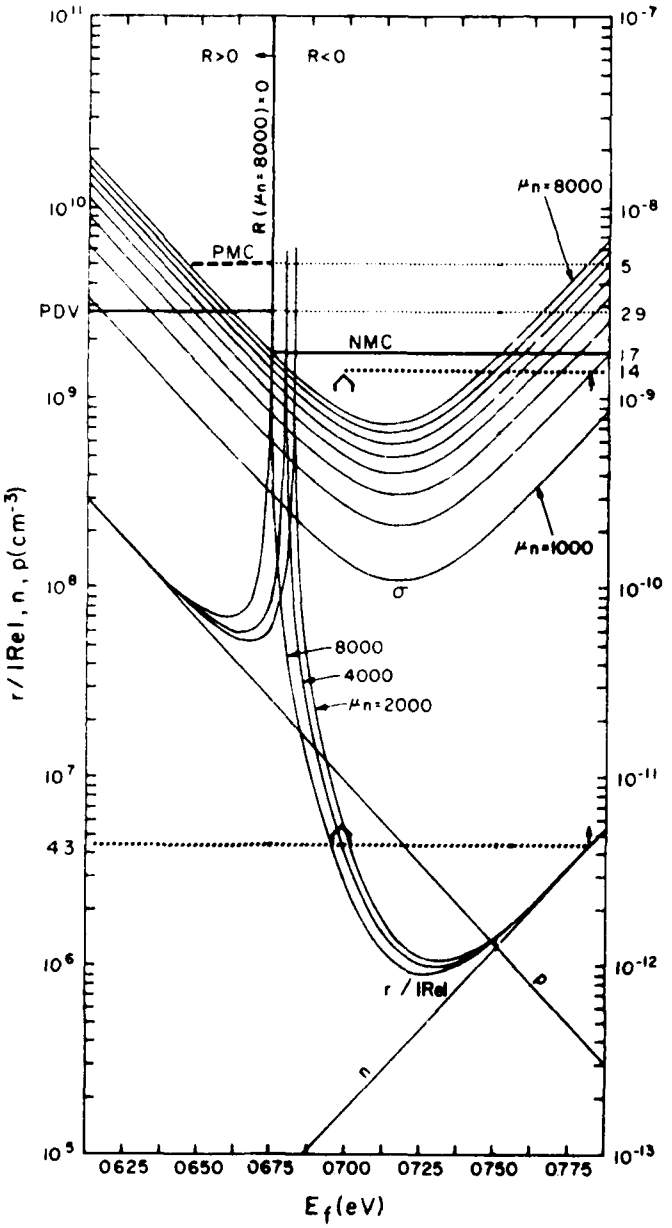

$T = 295K$

$N_c = 4.13 \times 10^{17} cm^{-3}$

$N_v = 8.41 \times 10^{18} cm^{-3}$

$E_g = 1.425 eV$

$$\frac{\mu_n}{\mu_p} = 13 + 0.0009\mu_n$$

$r_n = r_p = r$

$$\frac{r}{Re} = \frac{(n+pb^{-1})^2}{(n-pb^{-2})}$$

$$\sigma = \mu_n e(n+pb^{-1})$$

$$b = \frac{\mu_n}{\mu_p}$$

Figure 2. Carrier Concentrations, Hall Concentration and Conductivity vs. Fermi, T=295K.

Hall concentration and conductivity as functions of Fermi energy and the parameter electron mobility at 295K. Measurements from sample Cr2, Table 2, are analyzed.

dotted conductivity data line (2.4 X 10^{-5} S/cm) with these system Fermi levels (long arrows) at points Q1 and Q2 determine the conductivity curves, and thus the electron mobilities μ_n.

The conductivity curve that runs through Q1 has an electron mobility of about 3200 cm^2/Vs, that is, μ_H, as expected. Interpolation between curves can be carried out using equation (2) and the carrier concentrations implied by the system Fermi levels. Clearly, Q2 is well above the conductivity curve defined by the lattice-limited mobility and represents an inadmissible solution.

The conductivities of samples B1 and Cr2, displayed by the heavy horizontal dotted lines in Figures 1a and 2, respectively, are below the NMC lines of these figures and will be considered in the chapter on mixed conduction analysis, page 8.

For positive Hall coefficients, that is, for Fermi energies less than $E_f(R=0)$, the conductivity criterion PMC is higher with values of 2 X 10^{-5} and 5 X 10^{-9} Siemens/cm for 400K and 295K, respectively. The PMC line is determined by the intersection of the conductivity curve for the lattice-limited mobility with the "low-energy" border (LBMCR) of the MCR. The latter was chosen to exhibit the same deviation ($\sim$12%) of $r/|Re|$ from carrier concentration (here p) as obtained at the energy where n = p (the high-energy border of the MCR). (See Figures 1b and 2.)

As may be inferred from a review of the data of Table 1, for positive [illegible] coefficients, σ_p/σ is greater than 90% for b greater than 10.

TABLE 1. IMPORTANT CHARACTERISTICS OF THE ANALYSIS

Relative magnitudes which indicate the degree of mixed conduction at key po[illegible]n the NRMCR as a function of μ_n/μ_p. A scattering factor r of 1 is assumed.

	Lower Border		Conductivity Minima		Upper Border	
	R = 0				$E_f = E_{fi}$	
	$p/n = (\mu_n/\mu_p)^2$		$p/n = \mu_n/\mu_p$		p/n = 1	
μ_n/μ_p	σ/σ_p	μ_H/μ_n	σ/σ_n	μ_H/μ_n	σ/σ_n	μ_H/μ_n
16.6[a]	1.06	0.00	2.00	0.47	1.06	0.94
15.0	1.07	0.00	2.00	0.47	1.06	0.93
10.0[b]	1.10	0.00	2.00	0.45	1.10	0.90

a. 16.6 corresponds to μ_n of 4000 in equation 9.

b. Below minimum predictable μ_n of equation 9, but interesting for perspective.

Applications of Conductivity Criteria

The results of room-temperature measurements on ET&DL samples, together with a comparison of Look's old and new mixed conduction analyses with the present analysis, are displayed in Table 2. Samples U1-U4 are undoped, and both the present criterion for $R = 0$, ($\sigma > 2 \times 10^{-9}$ S/cm) and Look's new analysis indicate that mixed conduction effects are minimal, and n and μ_n are given by $(eR)^{-1}$ and $R\sigma$, respectively. The results of Look's old analysis differ from these conclusions and include predicted hole mobilities well over the lattice-limited value of 400 cm^2/Vs.

Look's new analysis,[3] which limited itself to room-temperature measurements of samples exhibiting negative Hall coefficients, established a minimum conductivity criterion of 2 to 2.5 $\times 10^{-9}$ S/cm for MC analysis. This agrees quite well with the criterion established by the minimum visible deviation of $r/|R|$ from n (2 to 2.5 $\times 10^{-9}$ S/cm) in Figure 2; the vertical dotted line defined by the 8% deviation of the Hall curve from linearity results in a conductivity criterion of 2×10^{-9} S/cm. Look's technique employs a family of curves relating μ_H to μ_n through the parameter resistivity, and is based on equations (1), (2), and (9) and a tentative value of n_i (2.6×10^{-6} cm^{-3}), determined as a best fit to measurements made at 295K. The value of n_i can be obtained either from the intersection of lines n and p in Figure 2, or from the following expression:

$$n_i = (np)^{1/2} = (N_c N_v \exp(-E_g/kT))^{1/2} \qquad (10)$$

where the effective densities of states, N_c and N_v, of Blakemore[14] are used to obtain $n_i = 1.25 \times 10^6$ cm^{-3} at 295K. Thus, the resulting conductivity criteria are not strongly dependent on the exact choice of n_i nor, as can be seen from Table 1, on the mobility ratio b. Table 1 shows that for mobility ratios b, as low as 10 μ_n is close to μ_H and σ_n to σ at the intrinsic Fermi level.

Dependence of Carrier Dominance on Fermi Energy

The three long solid lines in Figure 1b mark energies defined in Table 1. Because the $R = 0$ and $p = n$ lines are well-defined, easily recognizable, and are sufficiently close to the energies where discernible deviations of σ from linearity first occur, they are convenient borders for the region where neither carrier dominates conduction. These lines also separate regions of decreasing degrees of p-dominance arising with increasing Fermi energy. In the region where $R > 0$, complete p-dominance prevails; that is, the Hall effect conductivity and carrier concentration are all hole-dominated, and the sample is denoted as being p-type of the third degree, or ppp. In the intermediate region between $R = 0$ and the locus of the conductivity minima, $R < 0$ but $\sigma_p > \sigma_n$ and $p > n$, so we have p-dominance of the second degree, or ppn. The following region has as its upper bound the Fermi energy at which the n and p lines cross. Here we have $R < 0$ and $\sigma_p < \sigma_n$, but p is still greater than n, so that only first degree or p concentration dominance results and is denoted by pnn. In the region labeled nnn, $R < 0$ $\sigma_p < \sigma_n$ and $p < n$; thus, complete n-dominance prevails.

ANALYSIS OF MIXED CONDUCTION EFFECTS

For conductivities below the established criteria we will graphically solve equations (2), (3), (6), (7), and (8) or (9), simultaneously, to resolve the electron and hole concentrations and mobilities. The whole process may be considered equivalent to solving the following quartic equation for n and equations (6), (7)

TABLE 2. COMPARISON OF ANALYSES ON ROOM TEMPERATURE MEASUREMENTS

Mixed conduction analysis of room-temperature measurements on ET&DL samples. Results from Figure 2, as well as Look's old and new analyses, are compared. All analyses use a scattering factor r of 1.

	Measurements			Analysis From Fig. 2		Look's NEW ANALYSIS		Look's OLD ANALYSIS			
SAMPLE	$(eR)^{-1}$ ($10^6 cm^{-3}$)	σ (10^{-9}S/cm)	$\mu_H=R\sigma$ (cm^2/Vs)	n ($10^6 cm^{-3}$)	μ_n (cm^2/Vs)	n ($10^6 cm^{-3}$)	μ_n (cm^2Vs)	n ($10^6 cm^{-3}$)	μ_n (cm^2/Vs)	p ($10^6 cm^{-3}$)	μ_p (cm^2/Vs)
UNDOPED											
U1	-3.73	2.38	3970	3.73	3970	3.73	3970	2.12	5370	3.33	989
U2	-7.29	3.45	2970	7.29	2970	7.29	2970	2.74	5230	5.00	1470
U3	-12.4	2.13	1060	12.4	1060	12.4	1060	1.27	4750	3.50	2050
U4	-9.05	3.33	2300	9.05	2300	9.05	2300	-	-	-	-
Cr-DOPED											
Cr1	-3.90	1.33	2140	3.90	2140	3.90	2140	.959	4550	7.90	500
	-	-	-	-	-	.46	$6.5x10^3$	-	-	-	-
Cr2	-4.30	1.39	2020	4.30	2020	4.30 .42	2020 $6.8x10^3$	-	-	-	-

and (2), respectively, for E_f, p and μ_n:

$$(Reb^2)n^4 - (rb^2)n^3 + (Rebn_i^2)n^2 + (n_i^2 r)\, n + (Ren_i^4) = 0 \qquad (11)$$

As we shall see, some "programmed solutions" to equation (11) can be misleading, and it is always best to have a complete picture of the processes involved, as afforded by Figures 1 and 2.

Constant Mobility Ratio (Measurements Made at 400K)

Let us consider the simplest case first, that of equation (8) used at 400K by Martin.[4] According to Descartes' rule. equation (11) has two changes of sign, and therefore two real solutions. As indicated in equation (11), if b is constant, n and therefore E_f, is independent of μ_n or σ. Thus, there exists only one curve for R, as shown in Figure 1a, and a measurement of R immediately yields the double-valued solution for n, p (μ_H/μ_n, σ/σ_n from equations (4) and (5)) and the system Fermi levels. The conductivity curves, or equation (2), then yield the double solution for μ_n. Hall and conductivity data from Sample B1, Table 3, are analyzed in Figure 1a.

As can be seen from Figure 1b, the entire Hall curve to the left of its minimum lies in the NRMCR for negative values of R. Since one of the values for any ambiguous solution for a Hall measurement must lie on this portion of the curve, it must fall within the NRMCR. Thus, the maximum conductivity that can be related through a Fermi level to that value of R is defined by the intersection of the R= 0 line with the conductivity curve corresponding to the lattice-limited mobility. Since line NMC denoting this conductivity also intersects the maximum conductivity curve at the p = n line, the latter becomes the high energy border of the double solution region. Thus, NRMCR, defined earlier, also corresponds to the region for which there are two real solutions to the quartic. Hence, the rationale for the previously discussed p = n (or 12% deviation) criteria for mixed conduction becomes clear.

Examples of such double-valued solutions are represented by the short and long arrow pairs in Figure 1a for Samples B1 and C2, respectively. In each case, the sample Fermi level E_{FS} is found on the r/|Re| curve from the measured value of the Hall coefficient. The conductivity curve passing through the conjunction of E_{FS} with the measured conductivity then corresponds to the μ_n of the sample. Points P indicate the double-valued solution of μ_n for Sample B1, namely, μ_n = 2100 and 5200 cm^2/Vs, which satisfy the measured conductivity 2.7 X 10^{-6} at the two Fermi energies implied by the measurement of 1/|Re|. Similarly, points Q indicate the solutions for specimen C2, but, in this case, the solution corresponding to point Q2 would be well above the lattice-limited mobility and is, therefore, not admissible. Consideration of point Q2 is, of course, also ruled out by the conductivity criterion established above.

For positive Hall coefficients, two admissible solutions occur in the PRMCR for conductivities below line 1.1X10^{-5} S/cm in Figure1(where PDV is an abbreviation for positive double-value). However, significant MC effects on the approximation of r/|Re| to p continue to exist for conductivities as large as 2 X 10^{-5} S/cm or out to the Fermi energy labeled LBMCR. Therefore, the PDV line does not intersect the conductivity curve corresponding to the lattice-limited mobility at LBMCR, the lower border of both PRMCR and MCR. This means that the criterion for the onset of mixed conduction effects does not coincide with the criterion for the onset of double-valued solutions as it does for negative Hall coefficients.

Three analyses of Martin's measurements will be discussed, and the results, principally carrier concentration, will be listed in Tables 3 through 5. All involve the assumption that $\mu_n/\mu_p = 15$ and $r = 1$. The first analysis is based on Figure 1, the second on solution of equation (11) for the n_i (6.22×10^9 cm^{-3}) generated in Figure 1, and the third on solution of equations (2), (3), and (8) and use of Martin's estimate of $r\mu_n$, which he refers to as "electron mobility." The first two analyses should, but do not always, result in fair agreement. Unlike the first two, the third analysis results in only one solution for each set of measurements and a large spread in the n_i values. The average n_i is, however, in good agreement with the values deduced or assumed in the first two analyses.

Table 3 lists the two sets of solutions, including Fermi level and carrier concentrations implied by each individual Hall measurement, Figure 1, and the scattering coefficient r. The mobilities are then found from the conductivity measurement through use of interpolation in Figure 1 or equation (2) and the carrier concentrations.

The upper and lower sections of Table 1 reflect scattering factors of 1 and 1.26, respectively. The former is the convenient approximation typically[1-3] made, but is inconsistent with the measurements of samples A9, B2, and the $r/|Re|$ minimum of Figure 1. The latter both satisfies these data and is near the center of the estimated[8] range in r, 1.2 ± 20%. The solutions obtained for samples B1 and B3 for an r of 1.26 are listed to indicate the size of the changes in concentrations and mobilities resulting from this increase in scattering factor. The change for solutions inside the mixed conduction region is small, and, of course, this is the primary area of interest here. Outside the mixed conduction region, uncertainty in the scattering factor has a much greater effect on the estimation of μ_n from the $r\mu_n$ or μ_H data, such as Martin obtains from epilayer measurements.

Table 4 lists calculator-generated solutions of equation (11) based on the method of steepest descent.[15] Four solutions are generated, all are complex for $1/|Re| < 4.0 \times 10^9$; for $1/|Re| > 4.1 \times 10^9$ cm^{-3}, two are real and two are complex with comparable real and imaginary components. The amplitudes of the complex solutions are the same, unlike those of the real solutions. As the value of $1/|Re|$ approaches and drops below 4.0×10^9 cm^{-3}, the two real solutions merge and two complex solutions having the same real part emerge. As Figure 1 correctly indicates, this merger should occur as $1/|Re|$ drops below the minimum value of 5.06. This delay in "coupling" the real roots generated by the computer results in two real solutions for Sample B2 which fail to satisfy equation 3 for R.

Table 5 lists Martin's measurements and estimates of $r\mu_n$, as well as the resulting carrier concentrations and range of n_i determined for $r = 1$ from equations (2), (3), and (8). Using a knowledge of the concentrations of dominant dopants in his bulk material, together with a plot of electron-free carrier concentration vs. Hall mobility in very high-purity VPE samples, Martin estimated the electron mobility in his bulk samples. Samples A9 and A10 are dominated by deep donor-level (referred to as EL2) concentrations of a few 10^{16} cm^{-3}, and were estimated to have electron mobilities of 5000 cm^2/V. Samples B1 through B5 were dominated by chromium concentrations near 10^{17} cm^{-3}, and were estimated to have electron mobilities of 4000 cm^2/Vs. These estimates permitted deduction of the ratio $\mu_H/r\mu_n$ which, in turn, was used with b to deduce values for the concentration ratios $[EL2]/(N_A-N_D)$ and $[Cr]/([EL2] + N_A-N_D)$.

In a later paper,[16] Martin referenced results of Look's old mixed conduction analysis as evidence that $r\mu_n$ varies only slightly as a function of ionized impurity scattering, and as a rationale for treating $r\mu_n$ as constant at about 4000 cm^2/Vs. As shown in Table 5, the estimations from reference 4 imply a variable n_i ranging from 2.9 to 11 $\times 10^9$ cm^{-3}. Interestingly, the average n_i is 6.1, which

TABLE 3. ANALYSIS OF MARTIN's MEASUREMENTS USING FIGURE 1

Carrier concentrations and relevant ratios implied by Fig. 1 and Hall effect measurements from Ref. 4; and mobility determinations implied by these carrier concentrations and the associated conductivity measurements. Scattering factors, r, of 1.0 and 1.26 are used.

SAMPLE	MEASURED	IMPLIED BY FIGURE 1					MEASURED	IMPLIED BY FIG. 1 or Eq. 2 and E_f	
	$1/eR$	E_f	n	p	μ_H/μ_n	σ/σ_n	σ	μ_n	μ_p
	(10^9 cm^{-3})	eV	(10^9cm^{-3})	(10^9cm^{-3})	-	-	(10^{-6}cm)	cm^2/Vs	cm^2/Vs
				Analysis For r = 1					
A9[a]	-4.0[e]	Complex solutions		-	-	-	1.2	Complex solutions	
A10[a]	-11	0.758	10.4	3.74	0.975	1.02	4.6	2700	180
		0.683	1.20	33.0	0.310	2.87		8500[g]	567[g]
B1[b]	-8.5	0.748	7.75	5.00	0.960	1.04	2.7	2100	140
		0.688	1.37	28.2	0.380	2.37		5200	347
B2[b]	-4.5[e]	Complex solutions		-	-	-	2.3	Complex solutions	
B3[b]	-17	0.775	17.0	2.30	0.990	1.01	2.2	800	53
		0.676	0.96	40.4	0.214	3.80		3800	253
B4[b]	-28	0.792	28.0	1.40	1.00	1.00	1.6	360	24
		0.670	0.80	48.0	0.14	5.06		2500	167
B5[c]	+312	0.610	0.141	274	0.058[d]	130[d]	5.0	1700	113
		0.638	0.314	123	0.027	27.2		3650	243
				Analysis For r = 1.264					
A9[a]	-4.0[f]	0.714	2.89	13.4	0.748	1.31	1.2	2000	133
		0.714	2.89	13.4	0.748	1.31		2000	133
B1[b]	-8.5	0.758	10.2	3.80	0.97	1.02	2.7	1600	107
		0.684	1.20	32.0	0.31	2.80		5000	333
B2[b]	-4.5	0.728	4.40	8.90	0.87	1.14	2.3	2900	192
		0.701	1.98	19.5	0.58	1.66		4450	297
B3[b]	-17	0.783	21.4	1.80	0.99	1.91	2.2	650	43
		0.673	0.88	44.0	1.80	4.30		3600	240

a. LEC-grown crystal, undoped
b. Bridgeman-grown crystals, heavily doped with chromium
c. LEC-grown crystal, heavily doped with chromium
d. Of greater interest here are the μ_H/μ_p and σ/σ_p ratios of 0.88 and 1.01, respectively
e. Absolute value less than 5.06 cm^{-3} which is the minimum allowable value of $1/|Re|$ for parameters of Fig. 1
f. Corresponds to minimum value of $1.264/|Re|$ for parameters of Fig. 1
g. Larger than lattice-limited mobilities

TABLE 4. ANALYSIS OF MARTIN's MEASUREMENTS USING COMPUTER-GENERATED SOLUTION TO QUARTIC EQUATION 11

Calculator-generated solutions to equation 11 for r = 1 and n_i = 6.244 X 10^9 cm^{-3}. (Compare with electron concentrations in Table 3.

SAMPLE	$(eR)^{-1}$ ($10^9 cm^{-3}$)	Real n ($10^9 cm^{-3}$)
A9	-4	a. Complex b. Complex
A10	-11	a. 10.7 b. 1.05
B1	-8.5	a. 8.15 b. 1.18
B2	-4.5	a. 3.57 b. 1.87
B3	-17	a. 16.8 b. 0.89
B4	-28	a. 27.9 b. 0.76
B5	+312	a. 0.14[i] b. 0.32

i. The corresponding value of p is 278 x $10^9 cm^{-3}$.

TABLE 5. ANALYSIS OF MARTIN's MEASUREMENTS USING MARTIN's ESTIMATES OF ELECTRON MOBILITY

Carrier concentrations n, p, and n_i deduced from equations 2, 3, and 8; measurements of R and σ and Martin's estimate of $r\mu_n$ using r = 1.

SAMPLE	$r\mu_n$	$(eR)^{-1}$	σ	μ_H	n	p	n_i
	(cm^2/Vs)	$(10^9 cm^{-3})$	$(10^{-6} S/cm)$	(cm^2/Vs)	$(10^9 cm^{-3})$	$(10^{10} cm^{-3})$	$(10^9 cm^{-3})$
A9	5000	-4	1.2	1850	.61	1.3	2.9
A10	5000	-11	4.6	2600	3.2	3.9	11.0
B1	4000	-8.5	2.7	1950	2.2	3.0	8.2
B2	4000	-4.5	2.3	3200	2.9	1.0	5.4
B3	4000	-17	2.2	820	.90	3.8	5.9
B4	4000	-28	1.6	360	.37	3.2	3.4
B5	4000	312	5.0	100	.31	11.0	5.9

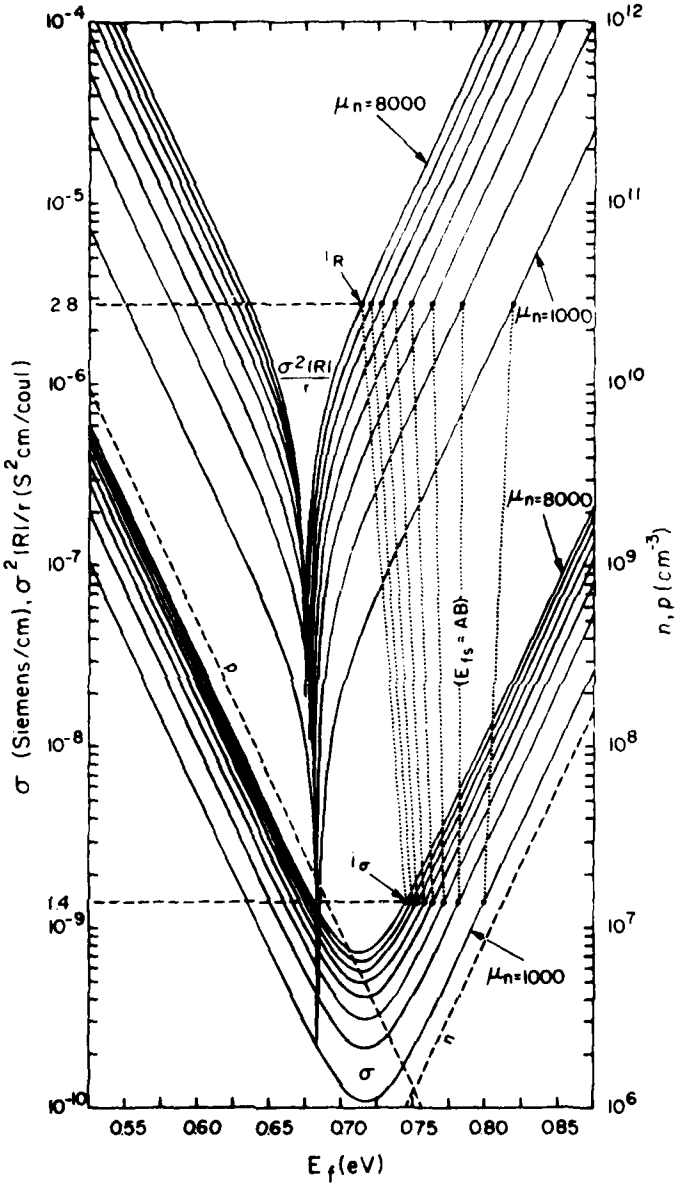

Figure 3. Carrier Concentrations, Conductivity and Conductivity Product vs. Fermi Energy as a Function of Electron Mobility, T=295K.

Measurement product, $\sigma\mu_H/r$ or σ^2R/r and conductivity as functions of Fermi energy, and the parameter electron mobility at 295K. Measurements from sample Cr2 are analyzed.

agrees well with the value 6.2 deduced from Figure 1. For three cases in Table 3, B3 and B5 (for r = 1) and B2 (for r = 1.264), the predicted values of $r\mu_n$ (which are in the MCR) agree reasonably well with the estimates made by Martin,[4] and fluctuations in such estimates are to be expected. Clearly, the establishment of a value for a fundamental quantity like the intrinsic carrier concentration at the temperature of interest is quite important, and the present analysis affords a useful vehicle for such considerations. (See, also, Blakemore.[14]) If we choose to assume values for the intrinsic carrier concentration and b, then the measurements of R and σ in Table 3 can be satisfied by two plausible solutions, both of which must be considered. In each case, one solution is outside the mixed conduction region, except for analyses of B2 and A9 for r = 1.26. In one case, A10, only the outer solution has a mobility below the lattice-limited value. We will consider later other techniques to permit discrimination between the ambiguous solutions.

Variable Mobility Ratio $b(\mu_n)$ (Measurements Made at 295K)

The above analysis of Figure 1 assumed a constant mobility ratio, b = 15, and produced a single curve based on the Hall coefficient which, in turn, depended only on E_f. In contrast, this analysis assumes a variable $b(\mu_n)$ of equation (9) to produce a family of such Hall curves which depend on μ_n or σ as well as on E_f. Figure 2 displays three members of this family of Hall curves for electron mobilities of 2000, 4000 and 8000 cm^2/Vs. The range in Fermi energy for this plot had to be reduced to half that of the other figures to permit clear display of three members of the family. For this reason, the $\sigma^2|R|$ plots of Figure 3 may be preferred for analysis. Unlike that for $1/|Re|$, these plots have a symmetry similar to that of the conductivity curves, and embody what is perhaps the simplest form for the relationship between the measured Hall coefficient and the transport properties

$$R\sigma^2/r = \mu_H\sigma/r = e\mu_n^2\ (pb^{-2}-n) \quad . \tag{12}$$

Either Figure 2 or Figure 3 can be used for mixed conduction analysis for the mobility ratio b of equation (9).

Figures 2 and 3 depict analyses of the conductivity and Hall measurements of sample Cr 2, Table 2. The solution entails determination of a mobility which allows satisfaction of both the conductivity and Hall coefficient measurements at the same Fermi level. The analysis in Figure 2 is simplified by the existence of a single $r/|Re|$ curve for energies above the MCR. Thus, the Fermi energy of the solution outside the MCR (single arrow) is uniquely determined by the Hall measurement; the mobility (about 2000 cm^2/Vs) is then implied by the conductivity. The broad arrow in the MCR indicates the ambiguity in the Fermi energy as determined solely from the $r/|Re|$ curves and measurement. It is immediately clear, however, from this broad arrow and the associated conductivity measurement, that the solution in the MCR implies mobilities above the lattice-limited values. Thus, even when a conductivity measurement implies an ambiguous solution, it is often rendered unique by this mobility consideration.

The technique for resolving an ambiguous, admissible solution (E_f and μ_n) in the MCR of Figure 2 is similar to that shown in Figure 3 for identifying a solution in any region. The dotted lines in Figure 3 illustrate this process for the same data used in Figure 2. These lines connect each σ^2R curve at the measured value with the curve of corresponding mobility at the measured conductivity. The vertical line A-B corresponds to the Fermi level associated with the solution. As with Figure 2, this analysis results in one solution which satisfies the measurement and mobility limitations. When there are two admissible solutions, one can turn to charge balance plots, thermopower, or other measurements described by Look[3] to

discriminate between solutions.

Look's new analysis admits of two solutions for each of the Cr-doped samples, Cr 1 and Cr 2, Table 2. In each of these cases, Figures 2 and 3 admit of only one solution and it is outside the mixed conduction region. The inconsistency in the results can only be attributed to the difference in n_i, chosen by Look as a best fit to his data and the value implied by Blakemore's[14] N_v. N_c values.

CHARGE BALANCE ANALYSIS

The Fermi level of any semiconductor is fixed by the necessity for charge conservation; that is, the number of electrons released from donors and the valence band must equal the number received by acceptors and the conduction band. This condition is expressed by:

$$\sum N_A^- + n = \sum N_D^+ + p \qquad (a)$$

where N_A^- and N_D^+ are the numbers of ionized acceptors and donors, respectively, which are given by:

$$(N_A^-, N_D^+) = \frac{(N_A,\ N_D)}{1 + (g_0/g_1)\ \exp\left(\{(E_A, -E_D) \mp E_f\}/kT\right)} \qquad (b)$$

Here we rely on Martin's work for the characterization of the Cr and EL2 levels. In particular, energy levels of 0.730 eV and 0.705 eV (measured from the valence band) are adopted for Cr and EL2, respectively. Martin found these values to be consistent with g_0, g_1 values of 0.93 and 1, respectively.

Condition (a) can be expressed graphically by plotting both sides of (a) against E_f on a semi-log plot, as done for Sample B3 in Figure 4. The Fermi level is determined by the intersection of $(\Sigma N_A^- + n)$ and $(\Sigma N_D^+ + p)$. This technique was introduced by Shockley[17] and has been used recently by others.[18-20] The conductivity curve for the deep Fermi level solution of Sample B3 and the Hall concentration curve are also drawn in on Figure 4 to permit comparison of the Fermi levels obtained using Figure 1a with that using Shockley diagram analysis.

Such comparisons permit resolution of ambiguous solutions even when impurity concentrations are known only approximately. For example, specimen B3 was lightly doped with Si to a concentration of about 3×10^{16} cm^{-3} and was estimated to have a similar EL2 concentration; B3 was doped to a Cr concentration of 3×10^{17} cm^{-3}. Since this is about 30 times greater than the total of all other acceptors, the point of intersection of the $(\Sigma N_A^- + n)$ curve and the $(\Sigma N_D^+ + p)$ curve is little affected by the inaccuracy of our estimate for the total shallow acceptor concentration for Fermi energies of interest here, e.g., those above the discontinuity in the Hall curve. Thus we obtain the estimate shown of the Fermi level as determined from the impurity concentration information. The deep and shallow Fermi levels labeled $E_f(H)$ and E'_F are determined by the intersections A and A', respectively, of the Hall measurement with the Hall curve. The relatively small displacement (0.005 eV) of the Fermi level, determined from impurity concentrations from the deep level solution at A, resolves the ambiguity in the dual value solution.

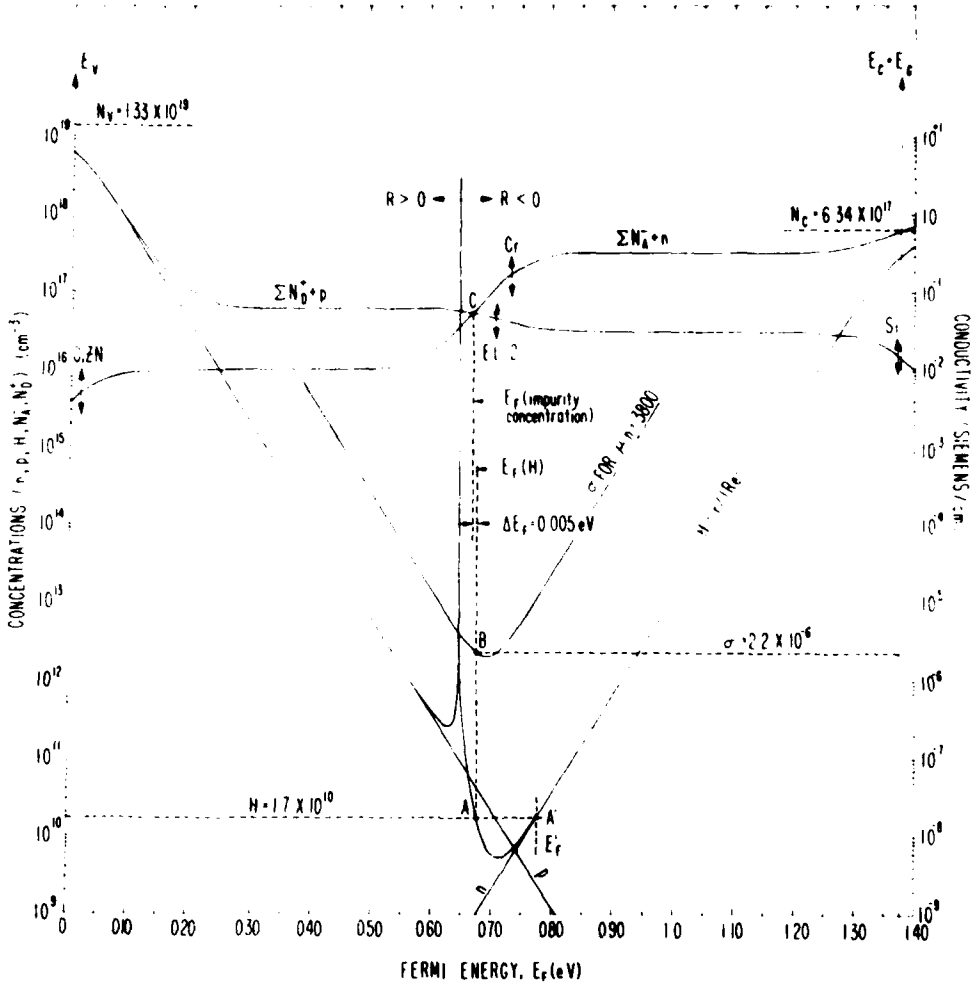

Figure 4. Charge Balance Plot

Charge balance plot representing the ionized impurity structure of Sample B3. Also shown are the conductivity curve representing the mobility associated with the deep Fermi level solution found using Figure 1a and the Hall concentration curve.

Conversely, if the Fermi level is known from the conductivity and Hall concentration analysis of Figure 1 (using other[3] electrical measurements to resolve any ambiguities), and if all the donor and the shallow acceptor concentrations are known, then the Cr concentration could be deduced using Shockley diagrams. More generally, the ramifications of changes in the relative impurity concentrations are subject to immediate visual inspection.

SUMMARY

We present an analysis of mixed conduction effects based on energy gap, recently deduced electron-to-hole mobility ratios used in related analyses, and newly revised calculations on the effective densities of states. Results of each of the analyses on appropriate data sets are compared. The technique presented permits consideration of charge-balance effects and impurity concentrations on the same graph, as well as the establishment of simple criteria for the necessity of mixed conduction analysis. This affords a means for immediate visual discrimination between double-valued solutions of carrier concentrations, or visual consideration of the impurity structure dominating compensation in the material.

ACKNOWLEDGMENTS

The authors express their appreciation to David Look for helpful discussions, and to William Hogelin for assistance in preparing this manuscript.

LITERATURE CITED

1. D. C. Look, "Mixed Conduction in Cr-Doped GaAs," J Phys Chem Solids 36, 1311 (1975).

2. D. C. Look, "The Electrical Characterization of Semi-Insulating GaAs," J Appl Phys, 48, 5141 (1977).

3. D. C. Look, "True Mobilities in Semi-Insulating O- and Cr-doped GaAs," Proceedings of the Semi-insulating III Materials Conf, Nottingham, England, Apr 1980, p. 183.

4. G. M. Martin, J. P. Forges, G. Jacob, and J. P. Hallaid, "Compensation Mechanisms in GaAs," J Appl Phys 51, 2840 (1980).

5. T. R. AuCoin, R. L. Ross, M. J. Wade, R. O. Savage, "Liquid Encapsulated Compounding and Czochralski Growth of Semi-insulating Gallium Arsenide," Solid State Technology 22, 59 (1979).

6. R. L. Ross, T. R. AuCoin, R. O. Savage, J. J. Winter, R. O. Malik, H. A. Leupold, and C. E. Anderson, Jr., "Growth and Characterization of Bulk Semi-insulating GaAs," ERADCOM Tech Rpt DELET-81, 12 May 1981.

7. M. Hemenger, "Measurement of High Resistivity Semiconductors Using the Van der Pauw Method," Rev Sci Instru 44, 698 (1980).

8. D. C. Look, "The Electrical Characterization of Semi-insulating GaAs," to be published. For lattice acoustical mode scattering and ionized impurity scattering, r is 1.18 and 1.93, respectively. For optical mode scattering, r may be obtained by a variational calculation (Reference 9) or an interactive solution of the Boltzman equation (Reference 10), and, typically, varies between

1.0 and 1.2 as a function of temperature (Reference 11). For a mixture of acoustic-mode and ionized-impurity scattering, r goes through a minimum value (Reference 12), dropping to about 1.05 at about 15% ionized impurity scattering. To summarize, r is difficult to calculate and even more difficult to measure, but it rarely varies by more than 20% from a value of 1.2.

9. H. Ehrenreich, Phys Rev 120, 1951 (1960).

10. D. L. Rode, Phys Rev B2, 1012 (1970).

11. G. E. Stillman, C. M. Wolfe, and J. O. Dimmock, J Phys Chem Solids 31, 1199 (1970).

12. S. B. Nam, Bull Amer Phys Soc 25, 43B (1980).

13. C. D. Thurmond, J Electrochem Soc 122, 1133 (1975).

14. J. Blakemore, J Appl Phys; to be published Jan 82.

15. J. B. Moore, "A Convergent Algorithm for Solving Polynomial Equations," J Assn Computing Machinery 14, 2 (1967).

16. G. M. Martin, "Key Electrical Parameters in Semi-Insulating Materials," Proceedings of the Semi-Insulating III-V Materials Conf, Nottingham, England, Apr 80, p. 13.

17. W. Shockley, "Electrons and Holes in Semiconductors," (D. VanNostrand Co., New York, 1950), p. 467.

18. H. A. Leupold, J. J. Winter, R. L. Ross, and T. R. AuCoin, "Analysis of Electrically Active Impurity Levels in In Situ Compounded Semi-Insulating GaAs," ERADCOM Tech Rpt, DELET-TR-81-7, Nov 80.

19. E. Spenke, "Electron Semiconductors," (McGraw-Hill Book Co., Inc., New York, 1958), p. 307.

20. R. Zucca, "Electrical Compensation in Semi-Insulating GaAs," J Appl Phys 48, 1987 (1977).

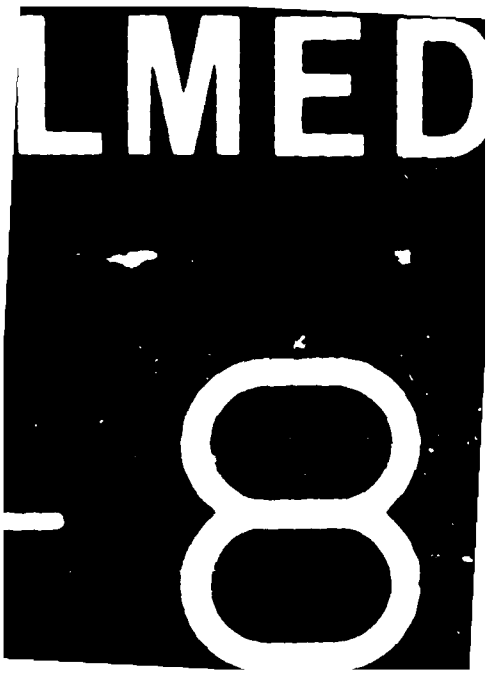
LMED
8